*Review (Invited)*

# Multimodal and *in-situ* Chemical Imaging of Critical Surfaces and Interfaces in Advanced Batteries

C-M. Wang,[1,3] P. Yan,[1] Z. Zhu,[1] M. H. Engelhard,[1] A. Devaraj,[2] B. L. Mehdi,[2] M. I. Nandasiri,[1] V. Shutthanandan,[1] Vijay Murugesan,[2, 3] and D. R. Baer[1,*]

[1]*Environmental Molecular Sciences Laboratory (EMSL) and* [2]*Physical and Computational Sciences Directorate, Pacific Northwest National Laboratory, 902 Battelle Boulevard, Richland, WA 99352, USA*

[3]*Joint Center for Energy Storage and Research, Argonne, Illinois 60439, USA*

** don.baer@pnnl.gov*

(Received: April 30, 2017; Accepted: October 26, 2017)

Interfaces play a critical role in the properties and lifetime of current generation and advanced batteries. However, detailed characterization of the critical interfaces during battery operation which can enable performance improvements and improved design has been a significant challenge requiring innovative technique development and creative experiments. This paper describes ways that information from a range of microscopy, spectroscopy, and spectrometry tools can be used to address important challenges associated with energy storage science and technology, in particular the development of advanced batteries for consumer use, transportation, and renewable storage. Expanding the types of measurements that can be made on operational model batteries has significantly expanded the type and quality of information that can be obtained. This paper first shows examples of approaches being used to collect *in situ* transmission electron microscopy (TEM), secondary ion mass spectrometry and x-ray photoelectron spectroscopy (XPS) data. The final section of the paper briefly shows two examples: the use of *in situ* XPS to examine solid-electrolyte interphase layers and a multimodal chemical imaging approach, including scanning TEM, atom probe tomography, scanning transmission x-ray microscopy, and x-ray adsorption near edge spectroscopy to understand the nanostructure and improve the performance of layered lithium transition metal oxide cathodes.

## 1. Introduction

Understanding reactions at interfaces plays a major role in the development of next generation batteries with longer lifetimes, higher capacity, lower cost and safe operation [1]. The performance and stability of electrodes and the nature of the solid-electrolyte interphase (SEI) layer when the electrolyte interacts with the electrodes are critical to battery performance and lifetime. Many analytical tools are being used to address the complex issues associated with electrode and electrolyte design, performance, and aging. Most commonly analytical tools have been used to examine batteries before and after a number of charge and discharge cycles. However significant advances in understanding the processes occurring in battery components are being facilitated through the use of tools that can examine batteries under battery operating conditions (*in situ* or *operando*) sometimes as a function of time and through the multimodal analysis using many different methods [2]. The Environmental Molecular Sciences Laboratory (EMSL) user facility is well positioned for developing *in situ* methods for analysis of many types of interface reactions including those occurring in batteries, during catalysis and even in biological systems. Such *in situ* methods currently include transmission electron microscopy (TEM) [3, 4], secondary ion mass spectrometry (SIMS) [5], X-ray photoelectron spectroscopy (XPS) [6], magnetic resonance – [nuclear magnetic resonance (NMR) and electron paramagnetic resonance (EPR)] [7, 8], and sum frequency generation (SFG) [9]. These methods provide a unique set of tools for learning more about the formation and properties of the SEI layer and behavior of elec-

trolytes during the battery cycling. Important roles remain for conventional and advanced *ex situ* methods to provide complementary information currently not available using *in situ* methods [2]. In order to collect important information both *in situ* and *ex situ* analysis methods require specialized analysis probes and/or careful sample handling in controlled environments.

The next section shows examples of some of methods for handling samples and making measurements in realistic or semi-realistic conditions. The following section provides recent examples of information that can be obtained using a multiple complementary and advanced methods.

## 2. *In situ* cells and sample handling

The analysis of working batteries or battery components by *in situ* and *in situ* real-time methods requires the design of uncommon methods to prepare a battery or set of battery components in such a manner that the regions of interest can be examined. In this section we briefly describe some *in situ* probes, sample cell designs and other approaches we have used to examine these materials for TEM, SIMS and XPS analysis.

The first concept used to create a miniature battery for *in situ* battery studies in a TEM is shown in Fig. 1[10]. This was an open cell battery for which the electrolyte was an ionic liquid with sufficiently low vapor pressure that the battery could be operated in the TEM without being enclosed. Although a number of quite interesting

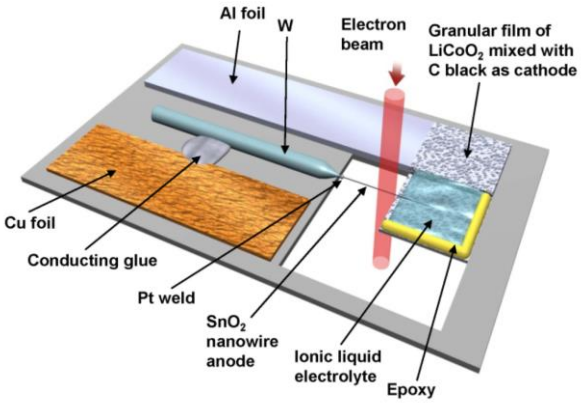


**Fig. 1.** (color online) Schematic drawing showing the fundamental concept of a lithium ion battery cell for in-situ TEM study of the battery under battery operating condition. The use of ionic liquid based electrolyte allows the direct loading of the cell into the TEM column and a single nanowire as anode lends the convenience of electron transparence for imaging. Adapted from reference [10].

results and publications were produced using open cells [11], ionic liquids and an open cell did not fully provide all the types of information desired and a closed cell was designed [11] as shown in Fig. 2a. Important features of this cell include the thin silicon nitride windows for enclosing the liquid and through which the electron beam can penetrate allowing a variety of TEM measurements [3, 12].

SIMS is also performed in ultra-high vacuum, conditions for which analysis of the solid-electrolyte interfaces

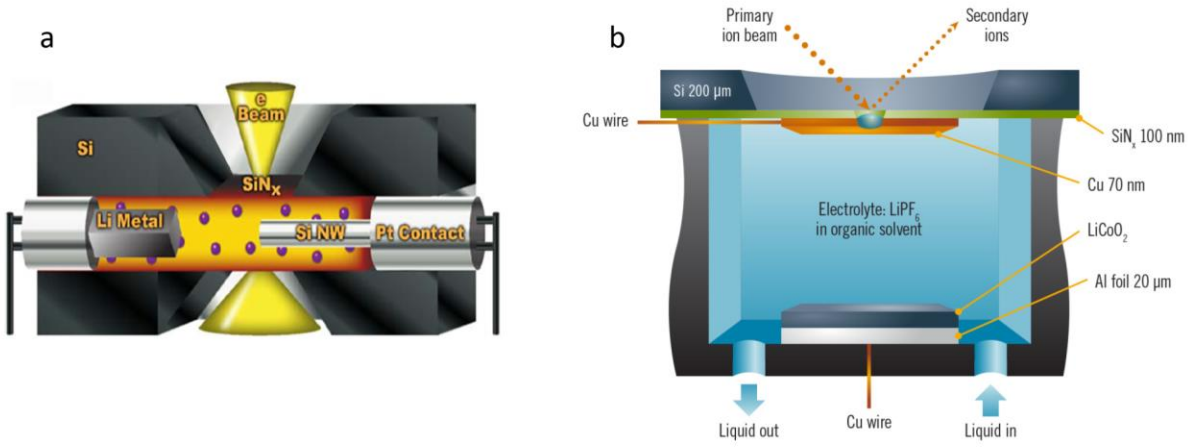


**Fig. 2**. (color online) Schematic illustrations of closed liquid cell for in-situ TEM and in-situ liquid SIMS study of the battery. (a) Closed cell for in-situ TEM, where a thin SiNx window is used to enclose the liquid electrolyte and allow electron beam transmit for imaging. (b) Closed cell for in-situ liquid SIMS, where the observable interface can be reached by bombarding through the membrane from the top. Figures adapted from references [2] and [11].

seems unlikely. However, a System for Analysis at the Liquid Vacuum Interface (SALVI)[13] allowing direct probing of liquid surfaces and interfaces by Time-of-Flight (ToF)-SIMS and scanning electron microscopy (SEM) enables SIMS to be used for a number of unexpected applications including electrochemical interfaces [5, 14] and biological systems[15]. The cell used for battery work (Fig. 2b) is in some ways similar to that used in the TEM studies in that it involves a silicon nitride window. However, the TEM cell needed to be thin to allow for electron transparency and the electron beam penetrated the cell. For SIMS, the silicon nitride window supports one of the electrodes. An ion beam is used to create a hole (~2 μm diameter) through the window, through the solid electrode and into the liquid electrolyte. The SIMS measurements can be taken while the battery is in different charge/discharge states. One interesting characteristic of SIMS is that the ion beam sputters through solid material, but molecular information can be collected near the surface of the liquid electrolyte [5].

We have found that XPS can be very important in understanding reactions occurring at electrode surfaces. Most of the XPS measurements involve disassembly of a battery in a controlled atmosphere glove box attached to an XPS spectrometer (Fig. 3). This approach, sometimes looking at battery components as a function of the number of cycles, is highly informative [16-23] but requires a new sample for each analysis condition.

Recently an open cell approach has been developed to look at the interactions of electrolytes with electrode surfaces as a function of bias condition[6]. A standard

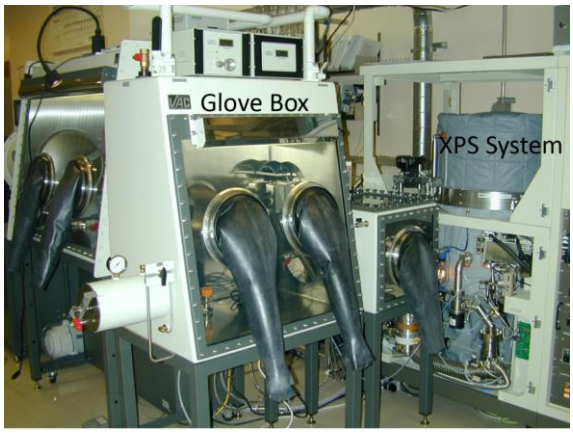


**Fig. 3.** (color online) Glove box attached to XPS system for anaerobic handling of battery components during and after disassembly in controlled environments in preparation for XPS measurements. Adapted from Ref. [2].

sample holder of the Kratos Axis Ultra XPS system has been modified to investigate the evolution of the SEI layer in Li-S battery systems under the normal operating conditions in the UHV environment. Fig.4 shows the top and side views of the modified sample holder where an anode, a cathode and an electrolyte of the Li-S cell are placed during these experiments. The electrodes are connected to the current carrying electrical feedthroughs on the XPS manipulator and utilized as leads for charging and discharging of the model battery using an external electrochemical analyzer. Because of S volatility, graphite was used as the cathode and Li metal as the anode. Both electrodes were mounted on a Teflon base for electrical isolation. A UHV friendly ionic liquid (IL) , 1-butyl-1-methylpyrrolidinium bis(trifloromethylsulfonyl) imide ($[bmpyr]^+[TFSI]^-$) was used as the co-solvent with

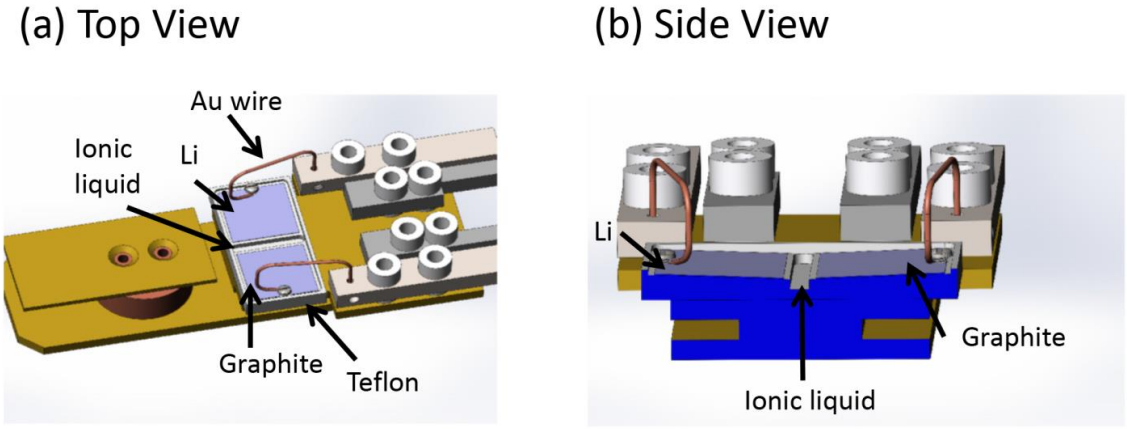


**Fig. 4.** (color online) Schematic diagram of the XPS sample holder developed for battery cycling and *in- situ* XPS characterization. Adapted from reference [6].

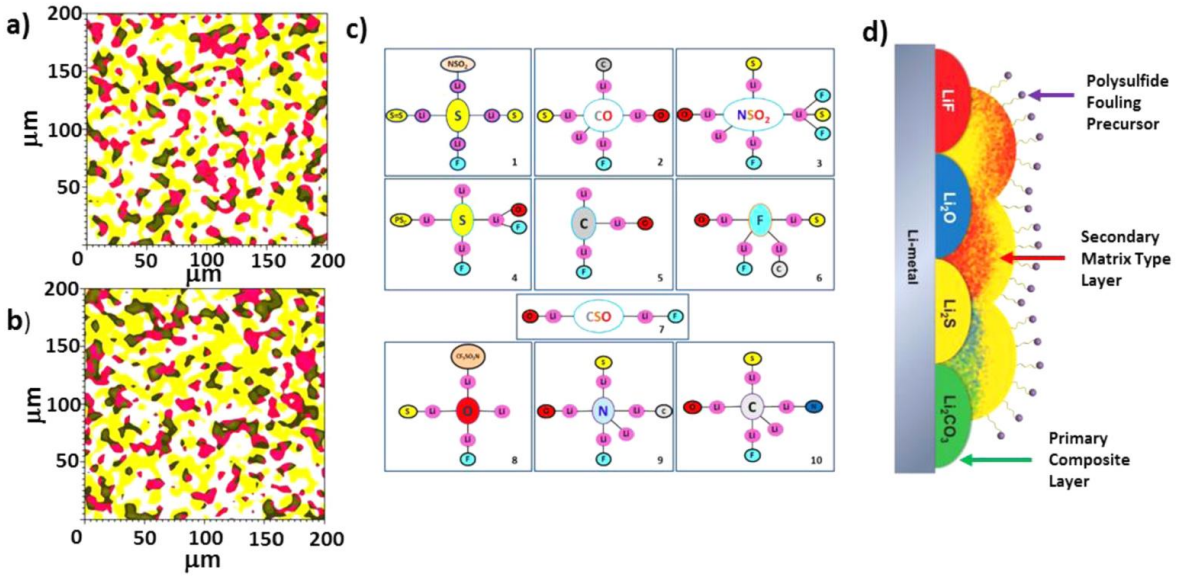


**Fig. 5.** (color online) (a) XPS chemical imaging of Li-electrolyte interfacial region after (a) first charging cycle (b) first discharge cycle. The Li-F species from F1s spectra and $S^0$polysulfide species from S 2p spectra are represented as yellow and red regions respectively. The black region represents the overlapping regions of Li-F and $S^0$polysulfide species. (c) Schematic representation of various fluorine based Li-F species predicted from AIMD calculations (d) cartoon representation of SEI layer growth mechanism based on our XPS and computational results. Adapted from reference [6].

1M $Li_2S_6$ dissolved in 1,3-dioxolane (DOL) and dimethoxyethane (DME) (20 wt.% relative to IL) as the electrolyte as well as the active redox material (polysulfides)[6] which was placed in the reservoir between the anode and cathode. The $Li_2S_6$ in the electrolyte acts as the active S material in Li-S cell and it resembles the initial discharge state of the battery. The IL provides the traditional TFSI counter anion and helps us study its role in SEI layer formation along with polysulfide species. In measurements reported in the next section the cell was fully charged and discharged at 2.2 V for two consecutive cycles. Measurements were performed at the end of each charge/discharge cycle to avoid the charge induced XPS peak shifts.

### 3. Example Measurements

Rather than duplicate information contained in reviews and summaries of TEM and XPS work [1, 3], in this section we summarize aspects of the new *in situ* XPS measurements, highlight the range of information can be obtained using a multi-technique analysis approach and provide an example of how careful TEM can be used to design a better electrode.

***In situ* XPS measurements and results** - Using the system and approached described above, C 1s, O 1s, F 1s and S 2p high resolution XPS spectra along with survey scans were collected before and after each cycle in a Kratos Axis Ultra DLD spectrometer. In addition, elemental and chemical state mapping were carried out in a field of view of 800 µm with a spatial resolution of ~ 5 µm. Density functional theory (DFT) was used to calculate the reaction energies for possible decomposition reactions of $Li_2S_6$ at the Li-anode and *ab initio* molecular dynamics (AIMD) simulation of the electrolyte mixtures in contact with a Li metal surface as described in our previous study [24] to investigate the SEI products generated from the decomposition of polysulfides and salt.

High resolution S 2p spectra included in ref [6] showed peak shifts associated with the formation of various sulfur compounds during charging and discharging. Three unique components were identified, namely sulfide dianion ($S^{2-}$) of $Li_2S$ at 160.2 eV along with terminal sulfur ($S_T^{1-}$) and bridging sulfur ($S_B^0$) of lithium polysulfide ($Li_2S_x$ with $x$>1) at 161.6 and 163.3 eV, respectively using careful peak fitting analysis. Detailed investigations indicated a shuttling process of polysulfide species during cycling resulting in eventual accumulation of $Li_2S$ and fouling of the Li-anode. These observations were in good agreement with AIMD analysis, which predicted the clustering of polysulfide chains in SEI layer. The

XPS analysis of C, O and F along with AIMD calculations also shed some insight into the electrolyte decomposition in the proximity of Li anode. XPS spectro-microscopy, as shown in Fig. 5a and b, was utilized to obtain the spatial distribution of concentration gradients associated with the SEI components. Compositional maps show that both $Li_2S$ and Li-F species form during the cycling process resulting in the precipitation of inorganic multiphase layer as the primary SEI component in addition to $Li_2O$ and $Li_2CO_3$. It appears that the reaction products of fluoride and sulfide anions engage in cross-interaction with adjacent electrolyte components due to the limited access to Li anode and generate a matrix type mixed SEI layer as shown in the cartoon picture (Fig.5d). Chemical entrapment of the dissolved polysulfides at the top layer on the Li-anode causes a fouling process and subsequent loss of active sulfur material and severe capacity fade as widely observed in Li-S battery technology. The measurements reported by Nandasiri et al [6] appear to be the first detailed in-situ XPS study of SEI layer evolution in Li-S batteries supported by AIMD. Further development and investigations are necessary to advance the capability to incorporate other material systems.

**Role of Ni in Li-rich lithium transition metal oxides as cathodes -** Nickel is one of the most popular and important elements in layered lithium transition metal oxide (LTMO) cathodes for lithium ion batteries. Ni acts as the cation redox specie during battery operation and can deliver two electrons by oxidizing a $Ni^{2+}$ cation to $Ni^{4+}$, thus facilitating a high capacity cathode. Moreover, the valence state change of Ni does not cause a Jahn-Teller distortion which is harmful to structural stability [25]. On one hand, introducing Ni into LTMO benefits the cycling performance; while on the other hand, it introduces challenges to materials design and stability. Taking Li-rich LTMO cathode as an example, Ni modifies not only the surface structure and chemistry of the particle but also the bulk lattice. Due to its high mobility in bulk lattice and its high catalytic effect to electrolyte, labile Ni-ions are believed to aggravate degradation of the material. We have applied a wide range of analytical methods to probe these materials before and after cycling as shown in Fig. 6. SEM TEM, scanning transmission x-ray microscopy (STXM), x-ray adsorption near edge spectroscopy (XANES) using the STXM beam and atom probe tomography (APT) data have been collected on the same particle. Each of the techniques has particular strengths and limitations. SEM provides a rapid image of the morphological features of the sample; TEM imaging combined with electron diffraction provides information about the material structure, which further can be combined with energy dispersive x-ray spectroscopy (EDS) to obtain information about elemental concentration and distribution in the sample. The spatially resolved XANES from STXM provides information about the chemical state and some aspects of elemental distribution in the sample [26, 27]. A particularly useful feature of APT is the ability to see light elements such as Li, which is more difficult to quantitatively analyze with TEM-EDS or electron energy loss spectroscopy (EELS) [28-30]. The full range of techniques can be used to examine material before and different material after cycling as shown for STXM and XANES data in Fig. 7. Ni

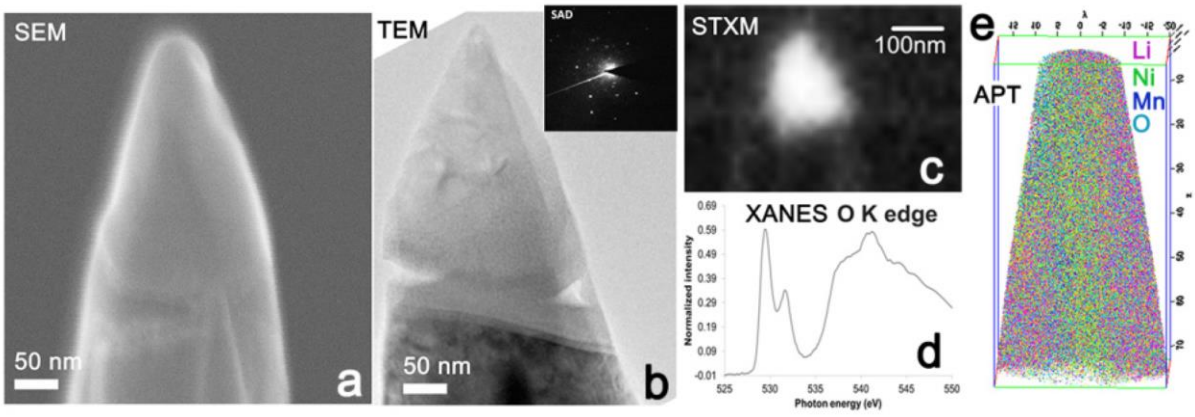


**Fig. 6.** (color online) The multimodal image shows the SEM, TEM, STXM, XANES and spatial distribution of elements captured by APT from the nanoparticle as shown by the SEM and TEM.

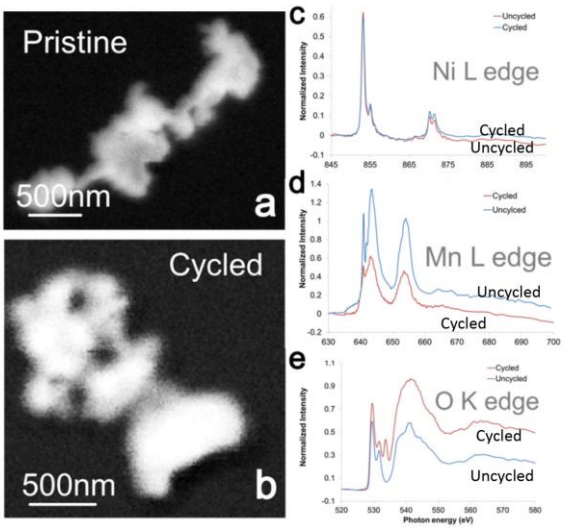


**Fig. 7**. (color online) The STXM figure shows the STXM map of $Li_{1.2}Ni_{0.2}Mn_{0.6}O_2$ cathode materials before and after cycling as well as the comparison of Ni, Mn L edge and O K edge of the pristine and cycled materials.

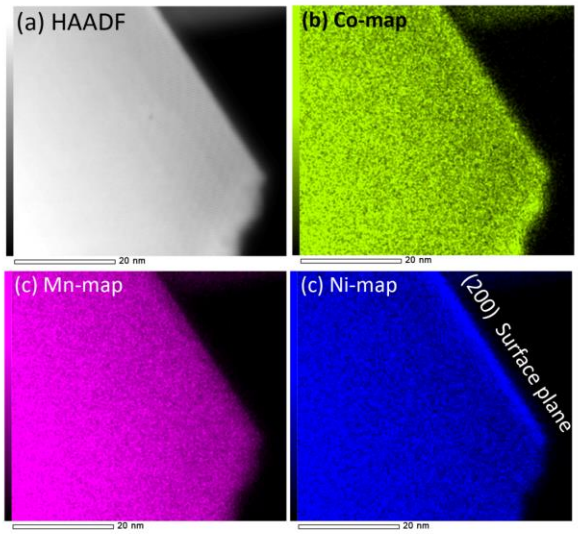


**Fig. 8.** (color online) a) HAADF STEM image and b) - d) STEM-EDS maps captured on a pristine cathode particle of $Li_{1.2}Mn_{0.54}Ni_{0.13}Co_{0.13}O_2$. The surface segregation of Ni is found only on the (200) surface plane.

L edge STXM maps of Li-rich LTMO cathode before and after cycling are given in (a) and (b) and corresponding Ni, Mn L-edge and O K-edge XANES spectra are given in (c-e). Such spatially resolved XANES and mapping permits identifying the location of oxidation state changes on electrodes induced due to cycling. Below the behavior of Ni in these cathode materials are examined in more detail, focusing on scanning TEM (STEM)-EDS measurements.

Fig. 8 shows low magnification STEM-EDS mapping on a pristine $Li_{1.2}Mn_{0.54}Ni_{0.13}Co_{0.13}O_2$ cathode particle, from which elemental surface segregation can be clearly seen. As shown in Fig. 8(b), the Co-map shows bright intensity near all surfaces, indicating higher Co concentration surface layer are formed. As indicated in Fig. 8(c), Ni enrichment is found only on the (200) surface, indicating Ni surface segregation is heavily influenced by crystallographic orientation. In the center of a grain, utilizing atomic resolution STEM-EDS mapping, we can directly visualize the differences on the elemental distri-

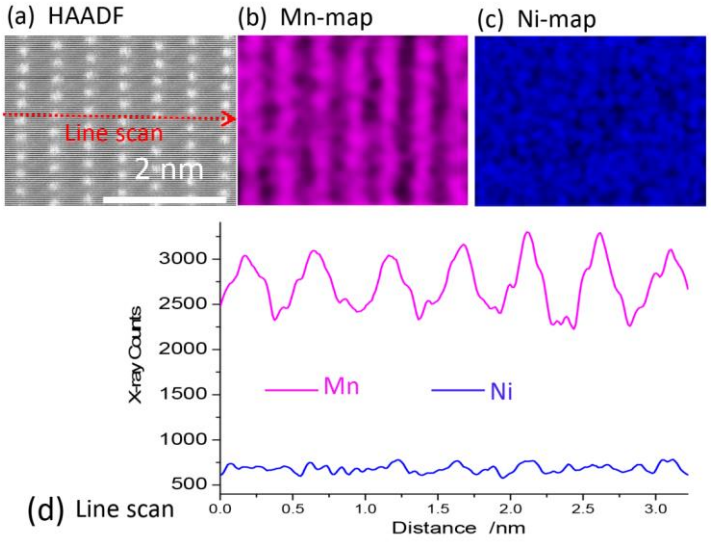


**Fig. 9.** (color online) Atomic resolution STEM-EDS maps captured on a pristine cathode particle of $Li_{1.2}Mn_{0.6}Ni_{0.2}O_2$. Mn-ions forms a well-ordered layered structure in (b), while Ni-map shows obvious interlayer mixing in (c). (d) shows integrated line scans perpendicular to the layers, where signals from Mn-map and Ni-map is clearly indicated.

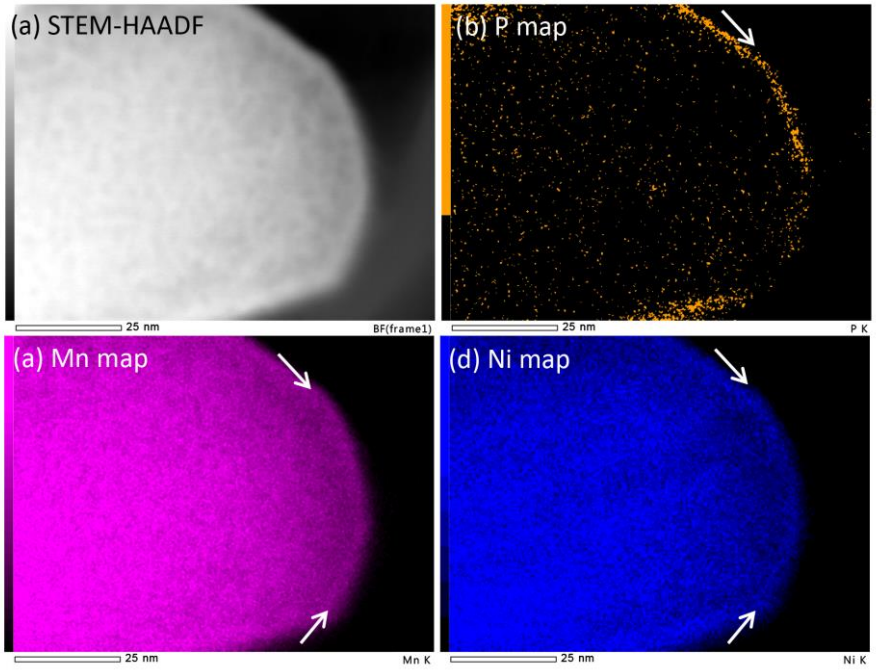


**Fig. 10.** (color online) STEM-EDS map captured on a cycled cathode particle of $Li_{1.2}Mn_{0.6}Ni_{0.2}O_2$. Due to cathode/electrolyte side reactions and cathode surface degradation, phosphorus, manganese, and nickel are enriched at particle surface as indicated by the white arrows.

bution between Mn and Ni. A STEM-high-angle annular dark-field (HAADF) images of the grain is shown in Fig. 9 (a). Corresponding elemental maps are shown in (b) and (c) for Mn and Ni, respectively. Fig. 9(b) shows a well ordered Mn structure while Fig. 9(c) does not show appreciable ordering for Ni, providing solid evidence that Ni has much higher Li/Ni interlayer mixing than Li/Mn [31]. This difference can be quantitatively shown by integrated line scans in a direction perpendicular to layer/row structure, as indicated by the dashed line in Fig. 9(a), The Ni signal does not show peaks because of anti-site mixing with the Li layer, leading to the randomized distribution [31, 32]. This data clearly demonstrates the elemental distribution differences for Mn and Ni.

Structural imaging and mapping of elemental distribution on the samples following the battery cycling provide insight as about the evolution of both structure and chemical composition as representatively shown in Fig. 10, where surface modifications after cycling were noticed. STEM-EDS mapping shows phosphorus, manganese and nickel are all enriched at particle surface in the cycled sample. Phosphorus is from Li-salt ($LiPF_6$) in the electrolyte, its appearance is a signature of electrolyte decomposition on cathode surface. Mn and Ni enrichment at surface are due to surface layer reconstruction, which causes unwanted cathode material degradation. It is worth pointing out that cycling induced Ni surface enrichment is different from the pristine Ni surface segregation; the former one has Ni concentrated on all surfaces but the latter one only appears on the (200) surface plane. This observation provides insights on how Ni behaves during the battery cycling. Firstly, as compared with Mn, Ni preferentially migrates to the Li layer. Also, following the migration of Ni to Li layer, it will irreversibly hop towards the particle surface, leading to a surface enrichment of Ni upon battery cycling. By virtue of advanced chemical imaging techniques, such as STEM-EDS, we are able to investigate the structure and chemistry of material from micrometer level down to atomic level, unveiling the structure-property relations for guiding material design and discovery for achieving better performance.

## 4. Conclusions

Over the past decade major progress has been made enabling important *in situ* real-time measurements. This has significantly changed the way that battery electrode concepts can be tested, providing important new information for advancing battery material development and

understanding aging and failure processes. However, it should be generally realized that the *in situ* microscopy and spectroscopy/spectrometry methods developed up to date remain far from realistic battery operating conditions. Some synchrotron based x-rays methods appear to get closer than other high vacuum based tools in the effort to move toward increasingly realistic conditions. However, many innovative concepts are still needed in the effort to understand actual battery functions in real-time. Developments will likely include new combinations of techniques with increasing the sensitivity, specificity and temporal resolution**.**

There still remains significant value for the use of *ex situ* and near *in situ* methods, especially when used in combination with information from the *in situ* real-time tools. This is particularly important because the sensitivity and detailed information available from well-developed *ex situ* methods generally exceeds those available when making *in situ* measurements in complex environments and at high temporal resolution. There is significant value in integrating information from an appropriate set of complementary methods. Care must be taken to handle and prepare specimens being analyzed without destroying the critical information and it is useful to carefully define the question being addressed or the process being examined or tested.

The integrated use of multiple techniques and real-time data collection require a range of research and technique expertise and present the need to process, analyze and store significant streams of data. Further, it should be realized that for analyzing processes at solid-liquid-gas interfaces, the seamless integration of ex-situ/in-situ experiments and theoretical modeling is required for pushing this field forward.

## 5. Acknowledgements

The topical work covered in this paper was enabled by the support of multiple programs centering on energy research including the Joint Center for Energy Storage Research, an Energy Innovation Hub funded by the Department of Energy (DOE), Office of Science, Basic Energy Sciences; the Assistant Secretary for Energy Efficiency and Renewable Energy, Office of Vehicle Technologies of DOE under Contract No. DE-AC02-05CH11231, Subcontract No. 6951379 under the advanced Battery Materials Research (BMR) program; and the Chemical Imaging Initiative, a Laboratory Directed Research and Development Program at Pacific Northwest National Laboratory (PNNL). Portions of the research were performed using the Environmental Molecular Sciences Laboratory, a national scientific user facility sponsored by the Department of Energy's Office of Biological and Environmental Research and located at PNNL. PNNL is a multiprogram national laboratory operated by Battelle for DOE under Contract DE-AC05-76RL01830. The STXM experiments were conducted at beamline 5.3.2.2 in the Advanced Light Source (ALS) facility at Lawrence Berkeley National Laboratory. AD acknowledges Dr. Craig Szymanski, Dr. Robert Colby and Dr. Suntharampillai Thevuthasan for their assistance to conduct STXM experiments. The ALS is supported by the DOE's Office of Science and Office of Basic Energy Sciences under Contract No. DE-AC02-05CH11231.

## 6. References

[ 1] M. Vijayakumar, Q. Luo, R. Lloyd, Z. Nie, X. Wei, B. Li, V. Sprenkle, J-D. Londono, M. Unlu, and W. Wang, *ACS Applied Materials & Interfaces*, **8**, 34327 (2016).

[ 2] C.-M. Wang, Z. Zhu, M. H. Engelhard, A. Devaraj, and D. R. Baer, *Microscopy Today*, **24(**2**),** 32(2016).

[ 3] M. Vijayakumar, N. Govind, B. Li, X. Wei, Z. Nie, S. Thevuthasan, V. Sprenkle, and W. Wang, *Frontiers in Energy Research*, **3**, 10 (2015).

[ 4] B. L. Mehdi, J. Qian, E. Nasybulin, C. Park, D. A. Welch, R. Faller, H. Mehta, W. A. henderson, W. Xu, C. M. Wang, J. E. Evans, J. Liu, J.-G. Zhang, K. T. Mueller, and N. D. Browning, *Nano Letters*, **15**, 2168 (2015).

[ 5] Z. H. Zhu, Y. F. Zhou, R. S. Vemuri, X. Wu, R. Zhao, X. L. Wang, S. Thevuthasan, D. R. Baer, and C. M. Wang, *Nano Letters*, **15**, 6170 (2015).

[ 6] M. I. Nandasiri, V. Shutthanandan, A. M. Schwarz, S. Thevuthasan, L. E. Camacho-Forero, P. B. Balbuena, K. T. Mueller, and V. Murugesan, *Chemistry of Materials*, **29**, 4728 (2017).

[ 7] W. Tang, Y. Liu, C. Peng, M. Y. Hu, X. Deng, M. Lin, J. Z. Hu, and K. P. Loh, *J. Am. Chem. Soc.*, **137**, 2600 (2015)..

[ 8] J. Xiao, J. Z. Hu, H. Chen, M. Vijayakumar, J. Zheng, H. Pan, E. D. Walter, M. Hu, X. Deng, J. Feng, B. Y. Liaw, M. Gu, Z. D. Deng, D. Lu, S. Xu,

C. Wang, and J. Liu, *Nano Letters*, **15**, 3309 (2015).

[ 9] L. Zhang, L. Fu, H.-f. Wang, and B. Yang, *Scientific Reports*, **7**, 44319 (2017).

[10] C. M. Wang, W. Xu, J. Liu, D. W. Choi, B. Arey, L. V. Saraf, J. G. Zhamg, Z. G. Yang, S. Thevuthasan, D. R. Baer, and N. Salmon, *J. Mater. Res.*, **25**, 1541 (2010).

[11] M. Gu, L. R. Parent, B. L. Mehdi, R. R. Unocic, M. T. McDowell, R. L. Sacci, W. XU, J. G. Connell, P. Xu, P. Abellan, X. Chen, Y. Zhang, D. E. perea, J. E. Evans, L. J. lauhon, J-G. Zhang, J. liu, N. D. Browning, Y. Cui, I. Arslan, and C-M. Wang, *Nano Letters*, **13,** 6106 (2013).

[12] L. Luo, P. Zhao, H. Yang, B. Liu, J.-G. Zhang, Y. Cui, G. Yu, S. Zhang, and C-M. Wang, *Nano Letters*, **15**, 7016 (2015).

[13] K. Y. Yu, D. Bufford, C. Sun, Y. Liu, H. Wang, M. A. Kirk, M. Li, and X. Zhang, *Nature Commun.*, **4,** 1377 (2013).

[14] Z. Wang, Y. Zhang, B. Liu, K. Wu, S. Thevuthasan, D. R. Baer, Z. Zhu, X.-Y. Yu, and F. Wang, *Anal. Chem.*, **89,** 960 (2017).

[15] X. Hua, C. Szymanski, Z. Wang, Y. Zhou, X. Ma, J. Yu, J. Evans, G. Orr, S. Liu, Z. Zhu, and X. -Y. Yu, *Integrative Biology*, **8**, 635 (2016).

[16] B. Liu, W. Xu, P. Yan, S. T. Kim, M. H. Engelhard, X. Sun, D. Mei, J. Cho, C. -M. Wang, and J. G. Zhan, *Advanced Energy Materials*, **7**, 1602605 (2017).

[17] D. Lu, J. Tao, P. Yan, W. A. Henderson, Q. Li, Y. Shao, M. L. Helm, O. Borodin, G. L. Graff, B. Polzin, C.-M. Wang, M. Engelhard, J.-G. Zhang, J. J. D. Yoreo, J. Liu, and J. Xiao, *Nano Letters*, **17**, 1602 (2017).

[18] T. Ma, G.-L. Xu, Y. Li, L. Wang, X. He, J. Zheng, J. Liu, M. H. Engelhard, P. Zapol, L. A. Curtiss, J. Jorne, K. Amine, and Z. Chen, *J. Phys. Chem. Lett.*, **8**, 1072 (2017).

[19] E. N. Nasybulin, W. Xu, B. L. Mehdi, E. Thomsen, M. H. Engelhard, R. C. Massé, P. Bhattacharya, M. Gu, W. Bennett, Z. Nie, C. Wang, N. D. Browning, and J.-G. Zhang, *ACS Applied Materials & Interfaces*, **6**, 14141 (2014).

[20] S. Song, W. Xu, R. Cao, L. Luo, M. H. Engelhard, M. E. Bowden, B. Liu, L. Estevez, C-M. Wang, and J-D. Zhang, *Nano Energy*, **33**, 195 (2017).

[21] S. Song, W. Xu, J. Zheng, L. Luo, M. H. Engelhard, M. E. Bowden, B. Liu, C-M. Wang, and J-G. Zhang, *Nano Letters*, **17**, 1417 (2017).

[22] F. A. Soto, P. Yan, M. H. Engelhard, A. Marzouk, C. Wang, G. Xu, Z. Chen, K. Amine,J. Liu,V. L. Sprenkle, F. El-Mellouhi, P. B. Balbuena, and X. Li, *Adv. Mater.*, **29**, 1606860 (2017).

[23] J. Zheng, M. H. Engelhard, D. Mei, S. Jiao, B. J. Polzin, J.-G. Zhang, and W. Xu, *Nature Energy*, **2**, 17012, (2017).

[24] L. E. Camacho-Forero, T. W. Smith, S. Bertolini, and P. B. Balbuena, *J. Phys. Chem. C* **119**, 26828 (2015).

[25] D. Kim, J. R. Croy, and M. M. Thackeray, *Electrochem. Commun.*, **36,** 103-106 (2013).

[26] A. Devaraj, C. Szymanski, P. Yan, C. Wang, V. Murgesan, J. Zheng, T. Tyliszczak, and S. Thevuthasan, *Microscopy and Microanalysis*, **21**, 685 (2015).

[27] W. C. Chueh, F. El Gabaly, J. D. Sugar, N. C. Bartelt, A. H. McDaniel, K. R. Fenton, K. R. Zavadil, T. Tyliszczak, W. Lai, and K. F. McCarty, *Nano Letters*, **13**, 866 (2013).

[28] A. Devaraj, M. Gu, R. Colby, P. F. Yan, C. M. Wang, J. M. Zheng, J. Xiao, A. Genc, J. G. Zhang, I. Belharouak, D. Wang, K. Amine and S. Thevuthasan, *Nature Commun.*, **6**, 8014 (2015).

[29] D. Mohanty, B. Mazumder, A. Devaraj, A. S. Sefat, A. Huq, L. A. David, E. A. Payzant, J. Li, D. L.Wood, C. Daniel, *Nano Energy*, **36**,76 (2017).

[30] A. Devaraj, D. E. Perea, J. Liu, L. M. Gordon, T. J. Prosa, P. Parikh, D. R. Diercks, S. Meher, R. P. Kolli, Y. S. Meng, and S. Thevuthasan, *International Materials Reviews*, **1**, (2017).

[31] P. Yan, J. Zheng, D. Lv, Y. Wei, J. Zheng, Z. Wang, S. Kuppan, J. Yu, L. Luo, D. Edwards, M. Olszta, K.l Amine, J. Liu, J. Xiao, F. Pan, G. Chen, J.-G. Zhang, and C.-M. Wang, *Chemistry of Materials*, **27**, 5393 (2015).

[32] P. Yan, J. Zheng, J-G. Zhang and C-M. Wang, *Nano Letters*, **17**, 3946 (2017).

**Discussions and Q&A with Reviewers**

**Reviewer #1 Satoshi Hashimoto (JFE Techno-Research)**

**[Q1_1]**

Although the distribution of F substance (LiF) is displayed in Fig. 5, it is not written from which material F is originated. Because F is an important element in the battery, the material is clearly shown.

**[A1_1]**

We appreciate the reviewers comments and careful reading of the manuscript and have responded to all of them. Responses to each of the reviewers comments are inserted below.

This issue arose because we attempted to simplify the discussion about the media used for the *in situ* XPS discussion. The Li is from LiF formed from decomposition of TFSI molecule { TFSI is (bis(trifluoromethane) sulfonamide - counter anion of Li-salt from electrolyte). We have expanded the description of the contents of the ionic liquid to include the TFSI. This was a good thing to be noticed by the reviewer.

**[Q1_2]**

Intensity of X-ray of Ni shown in Fig. 9 looks like rather weak, comparing with that of Mn.

Is the signal for Ni higher than that of noise level?

If the signal level is not enough larger, other data or idea are required to explain the distribution of Ni.

**[A1_2]**

The Ni signal is actually well above the noise for the EDX data, even though the signal is smaller than that for Mn. However, the Ni is moved around and not in necessarily expected positions, thus there are not the nice peaks indicating a well ordered lattice. We have addressed this in two ways. First we have added some words in one sentence and added a sentence in the discussion of Figure 9 and we have added two references that discuss this in more detail.

**Reviewer #2 Reviewer and Peer Review Content Private**